Journal of Computational and Applied Mathematics 368 (2020) 112479

Contents lists available at ScienceDirect

Journal of Computational and Applied Mathematics

journal homepage: www.elsevier.com/locate/cam

A lowest-order weak Galerkin finite element method for Stokes flow on polygonal meshes

Jiangguo Liu *, Graham Harper, Nolisa Malluwawadu, Simon Tavener

Department of Mathematics, Colorado State University, Fort Collins, CO 80523-1874, USA

ARTICLE INFO

Article history:
Received 6 April 2019
Received in revised form 5 September 2019

Keywords:
Discretely divergence-free
Lowest-order finite elements
Polygonal meshes
Stokes flow
Weak Galerkin

ABSTRACT

This paper presents a lowest-order weak Galerkin (WG) finite element method for solving the Stokes equations on convex polygonal meshes. Constant vectors are used separately in element interiors and on edges to approximate fluid velocity, whereas constant scalars are used on elements to approximate the pressure. For the constant vector basis functions, their discrete weak gradients are established in a matrix space that is based on the CW_0 space (Chen and Wang, 2017), whereas their discrete weak divergences are calculated as elementwise constants. To circumvent the saddle-point problem, a reduced scheme for velocity is established by using three types of basis functions for the discretely divergence-free subspace. A procedure for subsequent pressure recovery is also developed. Error analysis along with numerical experiments on benchmarks are presented to demonstrate accuracy and efficiency of the proposed new method.

1. Introduction

In this paper, we consider finite element solvers for two-dimensional Stokes flow in the velocity–pressure formulation

$$\begin{cases} -\mu\Delta\mathbf{u} + \nabla p = \mathbf{f} & \text{in } \Omega, \\ \nabla\cdot\mathbf{u} = 0 & \text{in } \Omega, \\ \mathbf{u} = \mathbf{g}, & \text{on } \partial\Omega, \end{cases} \tag{1}$$

where $\Omega \subset \mathbb{R}^2$ is a polygonal domain, $\mu > 0$ is the fluid kinematic viscosity, $\mathbf{u}$ the unknown fluid velocity, p the unknown pressure, $\mathbf{f}$ an external body force, $\mathbf{g}$ a boundary condition that satisfies the compatibility condition $\int_{\partial\Omega}\mathbf{g}\cdot\mathbf{n} = 0$ with $\mathbf{n}$ being the outward unit normal vector on the domain boundary $\partial\Omega$.

Development of efficient and robust finite element solvers for Stokes flow is a fundamental task in computational fluid mechanics. The classical finite elements [1–4], e.g., Taylor-Hood elements, focus on simplicial (triangular and tetrahedral) and (2-dim and 3-dim) rectangular meshes. Few work [5] addressed Stokes elements for quadrilaterals or other types of geometric shapes. It is recognized that there is a need for developing efficient and stable finite elements for Stokes problems on more general polygonal or polyhedral meshes.

Recently, the weak Galerkin (WG) methodology has demonstrated its potentials as a new platform for development of novel finite element methods for a wide range of scientific computing tasks [6–11]. Among the recent work on WG

* Corresponding author.
E-mail addresses: liu@math.colostate.edu (J. Liu), harper@math.colostate.edu (G. Harper), nolisa.malluwawadu@colostate.edu (N. Malluwawadu), tavener@math.colostate.edu (S. Tavener).

https://doi.org/10.1016/j.cam.2019.112479
0377-0427/

finite element methods for Stokes flow, [12,13] considered polygonal or polyhedral meshes in general and higher order polynomial approximants. In these cases, a penalty term is introduced to handle the discrepancy between the polynomials in element interiors and those on inter-element boundaries. However, it is possible to develop WG finite element methods on polygonal meshes and avoid the nonphysical penalty term.

In this paper, we develop a lowest-order WG finite element method for 2-dim Stokes flow problems on convex polygonal meshes. This can be viewed as a continuation of our previous efforts on developing lowest-order WG methods for Darcy flow and elasticity problems [8,14,15]. This also echoes the efforts in [16] for developing a simple WG method for Stokes flow on simplicial meshes. But the method in this paper applies to triangular, rectangular, quadrilateral, and more general polygonal meshes in a unified way.

The rest of this paper is organized as follows. Section 2 presents preliminaries on the Wachspress barycentric coordinates for polygons and the Chen-Wang CW_0 spaces that are $H(\mathrm{div})$-subspaces for polygons. Section 3 introduces the lowest-order weak Galerkin finite elements $(P_0^2, P_0^2; CW_0^2, P_0)$ for polygons. They are used to establish a numerical scheme in Section 4 for solving Stokes problems on polygonal meshes. Rigorous analysis for the numerical scheme is presented in Section 5. To overcome the saddle-point problems resulted from discretizing the Stokes equations, we investigate also construction of a discretely divergence-free subspace for velocity and subsequently pressure recovery in Section 6. Section 7 presents numerical experiments on four widely tested examples to demonstrate the accuracy and efficiency of our new method. Section 8 concludes the paper with some remarks.

2. Preliminaries

This section first presents preliminaries on Wachspress type barycentric coordinates for polygons and then briefly reviews the concepts, properties, and construction of the Chen-Wang spaces CW_0, which utilizes the Wachspress coordinates. The CW_0 spaces, as finite-dimensional $H(\mathrm{div})$-subspaces, are constructed for polygons [17], but can be viewed as extensions of the classical Raviart–Thomas spaces RT_0 for triangles and $RT_{[0]}$ spaces for rectangles.

2.1. Wachspress barycentric coordinates

The Wachspress coordinates extend the notion of barycentric coordinates for triangles to polygons [18].

Consider a typical convex polygon E with n vertices $\mathbf{a}_i (1 \le i \le n)$ that are arranged counterclockwise. Let $e_i (1 \le i \le n)$ be the edge that connects vertices $\mathbf{a}_i$ and $\mathbf{a}_{i+1}$. For convenience, we adopt the modulo n convention for indexing. So $\mathbf{a}_{n+1}$ is understood as $\mathbf{a}_1$. Let $\mathbf{n}_i (1 \le i \le n)$ be the outward unit normal vector on edge e_i. For $\mathbf{x} \in E^\circ$ (interior of E), its distance from $\mathbf{x} = (x, y)$ to edge e_i is

$$d_i = (\mathbf{a}_i - \mathbf{x}) \cdot \mathbf{n}_i, \quad 1 \le i \le n. \tag{2}$$

We introduce a scaled normal vector

$$\widetilde{\mathbf{n}}_i = \mathbf{n}_i / d_i, \quad 1 \le i \le n. \tag{3}$$

Then we define

$$w_i(\mathbf{x}) = \det(\widetilde{\mathbf{n}}_i, \widetilde{\mathbf{n}}_{i+1}), \qquad W(\mathbf{x}) = \sum_{i=1}^{n} w_i(\mathbf{x}). \tag{4}$$

Now we can define the Wachspress coordinates as

$$\lambda_i(\mathbf{x}) = w_i(\mathbf{x}) / W(\mathbf{x}), \quad 1 \le i \le n. \tag{5}$$

For a convex polygon, the Wachspress coordinates have the nice convexity and linear precision as stated in [18,19]:

$$\lambda_i(\mathbf{x}) \ge 0, \qquad \sum_{i=1}^{n} \lambda_i(\mathbf{x}) = 1, \qquad \sum_{i=1}^{n} \lambda_i(\mathbf{x}) \mathbf{a}_i = \mathbf{x}. \tag{6}$$

The standard barycentric coordinates for a triangle are linear functions. But the Wachspress coordinates are usually rational functions. As an example, we consider a convex quadrilateral E with vertices $(0, 0)$, $(1, 0)$, (a, b), and (c, d) (assuming counterclockwise orientation). For simplicity, we assume (a, b) is close to $(1, 1)$ and (c, d) is close to $(0, 1)$. The Wachspress coordinates are

$$\lambda_i(x, y) = f_i(x, y) / g(x, y), \qquad i = 1, 2, 3, 4, \tag{7}$$

where

$$\begin{cases} f_1(x,y) = ab + (b(b-1)-ab)x + (a(a-1)-ab)y \\ \qquad\qquad -b(b-1)x^2 + (2ab-a-b+1)xy - a(a-1)y^2, \\ f_2(x,y) = abx + b(b-1)x^2 - abxy, \\ f_3(x,y) = (a+b-1)xy, \\ f_4(x,y) = aby - abxy + a(a-1)y^2, \\ g(x,y) = ab + b(b-1)x + a(a-1)y. \end{cases}$$

When the quadrilateral degenerates into the unit square, i.e., $a = 1, b = 1, c = 0, d = 1$, the Wachspress coordinates become the familiar bilinear polynomials:

$$\lambda_1 = (1-x)(1-y), \quad \lambda_2 = x(1-y), \quad \lambda_3 = xy, \quad \lambda_4 = (1-x)y.$$

Further illustrative graphics about the Wachspress coordinates can be found in [8].

To facilitate the discussion, we utilize an auxiliary ratio function [19]:

$$\mathbf{R}_i(\mathbf{x}) = \frac{\nabla w_i(\mathbf{x})}{w_i(\mathbf{x})}, \quad 1 \le i \le n. \tag{8}$$

The quotient rule of differentiation yields

$$\nabla\lambda_i(\mathbf{x}) = \lambda_i(\mathbf{x})\Big(\mathbf{R}_i - \sum_{j=1}^{n} \lambda_j \mathbf{R}_j\Big), \quad 1 \le i \le n. \tag{9}$$

For later use, we also consider rotation of the gradient vector clockwise by 90°:

$$\mathrm{curl}(\lambda_i) = \begin{bmatrix} -\partial_y\lambda_i \\ \partial_x\lambda_i \end{bmatrix} = \begin{bmatrix} 0 & -1 \\ 1 & 0 \end{bmatrix} \nabla\lambda_i, \quad 1 \le i \le n. \tag{10}$$

2.2. $H(div)$-conforming CW_0 spaces for polygons

The $H(\mathrm{div})$-conforming CW_0 spaces constructed in [17] for convex polygons have attractive approximation properties.

We consider a typical convex polygon E with n vertices $\mathbf{a}_i (1 \le i \le n)$ that are arranged counterclockwise. Let $\mathbf{x}_c = (x_c, y_c)$ be the element center and $|E|$ be its area. For $1 \le i \le n$, let $|e_i|$ be the edge length and $\mathbf{n}_i$ the outward unit normal vector. Let $|T_i| (1 \le i \le n)$ be the area of the triangle formed by $\mathbf{x}_c, \mathbf{a}_i, \mathbf{a}_{i+1}$. Note we have adopted the modulo n notations for indexing.

As discussed in [8,17], we use these coefficients:

$$a_i = |e_i|/(2|E|), \quad 1 \le i \le n, \tag{11}$$

$$b_{i,j} = \delta_{i,j}|e_j| - |e_i||T_j|/|E|, \quad 1 \le i,j \le n, \tag{12}$$

$$c_{i,j} = -\frac{1}{n}\sum_{k=1}^{n-1} k\, b_{i,j+k}, \quad 1 \le i,j \le n, \tag{13}$$

where $\delta_{i,j}$ is the Kronecker symbol. It is shown in [17] that for any $1 \le i,j \le n$,

$$\sum_{k=1}^{n} b_{i,j+k} = 0, \qquad b_{i,j} = c_{i,j} - c_{i,j+1}.$$

Basis for CW_0 space. With the above coefficients, it is shown in [17] that the following n vector-valued functions form a basis for CW_0:

$$\mathbf{w}_i = a_i(\mathbf{x} - \mathbf{x}_c) + \sum_{j=1}^{n} c_{i,j}\,\mathrm{curl}(\lambda_j), \quad 1 \le i \le n, \tag{14}$$

where λ_j are the Wachspress coordinates (See Section 2.1).

Clearly, the basis functions in (14) rely on the frame consisting of the following $(n+1)$ functions

$$\mathbf{x} - \mathbf{x}_c, \quad \mathrm{curl}(\lambda_j) \ (1 \le j \le n),$$

which use the normalized coordinates and the Wachspress coordinates. The coefficients a_i, $c_{i,j}$ in (14) form a conversion matrix with rank n.

The reader is referred to [8] for graphics illustrating the CW_0 basis functions.

The CW_0 basis functions have theses noticeable properties:

$$\mathbf{w}_i|_{e_j}\cdot\mathbf{n}_j = \delta_{i,j}, \qquad \nabla\cdot\mathbf{w}_i = 2a_i, \qquad \forall 1\le i,j\le n. \tag{15}$$

So both pointwise normal fluxes and divergences are constants. The 1st item was established in [17]. The 2nd item can be derived from the fact that divergence of curl is zero. These properties set up the foundation for the CW_0^2 space (a matrix space based on the CW_0 space) to be used for Stokes flow.

3. WG(P_0^2, P_0^2; CW_0^2, P_0) finite elements for polygons

In this section, we first extend the CW_0 spaces of vector-valued functions to CW_0^2 spaces of matrix-valued functions. Then we discuss WG(P_0^2, P_0^2)-type discrete weak functions and define their discrete weak gradients in the CW_0^2 spaces and their discrete weak divergences as elementwise constants.

CW_0^2 **spaces for polygons**. Let E be a polygon. The $CW_0^2(E)$ space consists of the size 2×2 matrix-valued functions whose row vectors are in $CW_0(E)$. The properties in (15) imply the following

Lemma 0. *For any $W\in CW_0^2(E)$,*

(i) its classical divergence $\nabla\cdot W$ is a constant vector on E;
(ii) its trace $W\mathbf{n}$ is also a constant vector on each edge of E.

WG(P_0^2, P_0^2; CW_0^2, P_0) **finite elements for polygons**. Similarly to [14], we consider WG(P_0^2, P_0^2)-type vector-valued discrete weak functions on a polygon E with n edges. Such a function $\mathbf{v}=\{\mathbf{v}^\circ,\mathbf{v}^\partial\}$ has two parts: $\mathbf{v}^\circ$ denotes its value as a constant vector in the element interior E°; $\mathbf{v}^\partial$ denotes its value on the element boundary E^∂, which is a constant vector on each edge of the boundary. We can choose $2+2n$ basis functions are as follows.

- For the interior E°, there are 2 basis functions $\mathbf{v}_1$, $\mathbf{v}_2$. They can be chosen so that their values in the element interior are $\mathbf{v}_1^\circ=[1,0]^T$, $\mathbf{v}_2^\circ=[0,1]^T$. However, their values $\mathbf{v}_1^\partial$, $\mathbf{v}_2^\partial$ on the boundary E^∂ are the zero vector.
- For the ith ($1\le i\le n$) edge, we can choose 2 basis functions $\mathbf{v}_{2i+1}$, $\mathbf{v}_{2i+2}$ such that $\mathbf{v}_{2i+1}^\partial=[1,0]^T$, $\mathbf{v}_{2i+2}^\partial=[0,1]^T$ on the edge itself, but their values are the zero vector on all other edges and also in the element interior.

Here we remark that for the ith ($1\le i\le n$) edge, we can also use its unit normal vector $\mathbf{n}_i$ and unit tangential vector $\mathbf{t}_i$. In other words, $\mathbf{v}_{2i+1}^\partial=\mathbf{n}_i$ and $\mathbf{v}_{2i+2}^\partial=\mathbf{t}_i$ ($1\le i\le n$).

Let $\mathbf{v}=\{\mathbf{v}^\circ,\mathbf{v}^\partial\}$ be a WG(P_0^2, P_0^2)-type discrete weak function. We specify its *discrete weak gradient* $\nabla_w\mathbf{v}$ in $CW_0^2(E)$ via integration by parts

$$\int_E(\nabla_w\mathbf{v}):W=\int_{E^\partial}\mathbf{v}^\partial\cdot(W\mathbf{n})-\int_{E^\circ}\mathbf{v}^\circ\cdot(\nabla\cdot W),\quad \forall W\in CW_0^2(E), \tag{16}$$

where : is the standard colon product for matrices and $\mathbf{n}$ is the outward unit normal vector on the element boundary E^∂. If we set $\nabla_w\mathbf{v}=\sum_{j=1}^{2n}c_jW_j$, then the coefficients $c_1,\ldots,c_{2n}$ are readily available by solving a SPD linear system.

The *discrete weak divergence* $\nabla_w\cdot\mathbf{v}$ of such a discrete weak function $\mathbf{v}$ is also defined through integration by parts

$$\int_E(\nabla_w\cdot\mathbf{v})w=\int_{E^\partial}\mathbf{v}^\partial\cdot(w\mathbf{n})-\int_{E^\circ}\mathbf{v}^\circ\cdot(\nabla w),\quad \forall w\in P_0(E). \tag{17}$$

Note that the 2nd term on the right side of the above equation actually disappears, since the classical gradient of a constant function is a zero vector. Therefore, the discrete weak divergence can be computed directly.

4. Lowest-order WG scheme for Stokes flow on polygonal meshes

In this section, we develop a novel finite element scheme in the weak Galerkin framework for Stokes problems on polygonal meshes. The scheme uses the lowest-order approximants, namely, constant vectors for velocity and constant scalars for pressure.

Let $\mathcal{E}_h$ be a shape-regular convex polygonal mesh [8,10]. We use $\mathbf{V}_h$ to denote the space of the (P_0^2, P_0^2)-type discrete weak vector-valued functions defined on $\mathcal{E}_h$. Note that such a finite element shape function takes a constant vector value in the interior of each polygon and also a constant vector value on each edge of the mesh skeleton. It is obvious that

$$\dim(\mathbf{V}_h)=2\,(\#\text{elements}+\#\text{edges}).$$

We define $\mathbf{V}_h^0$ as a subspace of $\mathbf{V}_h$ consisting of functions that vanish on the boundary edges. We define W_h as the space of piecewise constants on $\mathcal{E}_h$. Clearly,

$$\dim(W_h)=\#\text{elements}.$$

Definition 1 (*Local L^2-projection Operators*)**.** Let E be a polygon. We define

(i) Q_h as the L^2-projection from $L^2(E)$ to the space of constant scalars on E;
(ii) $\mathbf{Q}_h = \{\mathbf{Q}_h^\circ, \mathbf{Q}_h^\partial\}$, where $\mathbf{Q}_h^\circ$ is the local L^2-projection from $L^2(E^\circ)^2$ to the space of constant vectors in E°, whereas $\mathbf{Q}_h^\partial$ is the local L^2-projection from $L(E^\partial)^2$ to the space of constant vectors on E^∂;
(iii) $\mathbb{Q}_h$ as the local L^2-projection from $L^2(E)^{2\times 2}$ to the matrix space $CW_0^2(E)$.

We define bilinear and linear forms for $\mathbf{u}_h, \mathbf{v} \in \mathbf{V}_h$ and $p_h \in W_h$ as follows

$$\mathcal{A}_h(\mathbf{u}_h, \mathbf{v}) = \sum_{E\in\mathcal{E}_h} (\nabla_w \mathbf{u}_h, \nabla_w \mathbf{v})_E, \tag{18}$$

$$\mathcal{B}_h(p_h, \mathbf{v}) = \sum_{E\in\mathcal{E}_h} (p_h, \nabla_w \cdot \mathbf{v})_E. \tag{19}$$

$$\mathcal{F}_h(\mathbf{v}) = \sum_{E\in\mathcal{E}_h} (\mathbf{f}, \mathbf{v}^\circ)_E. \tag{20}$$

For convenience, when $q \in W_h$, we consider also $\mathcal{B}_h(q, \mathbf{u}_h) = \sum_{E\in\mathcal{E}_h} (q, \nabla_w \cdot \mathbf{u}_h)_E$.

Scheme I. Seek $\mathbf{u}_h \in \mathbf{V}_h$ such that $\mathbf{u}_h|_{\Gamma_h^D} = \mathbf{Q}_h^\partial(\mathbf{u}_D)$ and for any $\mathbf{v} \in \mathbf{V}_h^0$, $q \in W_h$, there holds

$$\begin{cases} \mathcal{A}_h(\mathbf{u}_h, \mathbf{v}) - \mathcal{B}_h(p_h, \mathbf{v}) &= \mathcal{F}_h(\mathbf{v}), \\ \mathcal{B}_h(q, \mathbf{u}_h) &= 0. \end{cases} \tag{21}$$

To implement the above full scheme, one can use

- two natural basis functions $[1, 0]^T$, $[0, 1]^T$ for the interior of each element;
- again two natural basis functions $[1, 0]^T$, $[0, 1]^T$ on each edge, or equivalently the unit normal and tangential vectors $\mathbf{n}_e$, $\mathbf{t}_e$ for each edge e.

Anyway, the resulting discrete linear system has a size (3#elements + 2#edges). It is a typical saddle-point problem.

5. Error analysis

This section presents a complete rigorous error analysis for the WG finite element scheme developed in the previous section. We assume $\mathcal{E}_h$ is a shape-regular convex polygonal mesh. Finite dimensional subspaces $\mathbf{V}_h$, $\mathbf{V}_h^0$, W_h are all defined as in the previous section.

5.1. Lemmas on two semi-norms

Definition 2 (*Two Semi-norms on $\mathbf{V}_h$*)**.** For any $\mathbf{v} \in \mathbf{V}_h$, we define two semi-norms as follows

$$|\!|\!|\mathbf{v}|\!|\!|_1^2 = \mathcal{A}_h(\mathbf{v}, \mathbf{v}) = \sum_{E\in\mathcal{E}_h} \|\nabla_w \mathbf{v}\|_E^2, \tag{22}$$

$$|\!|\!|\mathbf{v}|\!|\!|_h^2 = \sum_{E\in\mathcal{E}_h} h_E^{-1} \|\mathbf{v}^\partial - \mathrm{tr}(\mathbf{v}^\circ)\|_{E^\partial}^2. \tag{23}$$

Remarks.

(i) Here $\mathrm{tr}(\mathbf{v}^\circ)$ means that we extend the constant vector value of $\mathbf{v}^\circ$ to the boundary E^∂ for each polygon E.
(ii) It is clear that $|\!|\!|\cdot|\!|\!|_1$ is based on the discrete weak gradient, whereas $|\!|\!|\cdot|\!|\!|_h$ involves another type of gradient in the discrete sense [14]. In the following, we shall show that these two semi-norms are equivalent.

Lemma 1 (*Commuting Identities*)**.** *Let E be a polygon. Then*

(i) For $\mathbf{u} \in \mathbf{H}^1(E)$, there holds $\nabla_w(\mathbf{Q}_h\mathbf{u}) = \mathbb{Q}_h(\nabla\mathbf{u})$;
(ii) For $\mathbf{u} \in H(div, E)$, there holds $\nabla_w \cdot (\mathbf{Q}_h\mathbf{u}) = Q_h(\nabla \cdot \mathbf{u})$.

Proof. These identities can be proved by using the definitions of the discrete weak gradient and discrete weak divergence, the definitions of the above local L^2-projections, and Gauss Divergence Theorem. □

Lemma 2 (*Conversion to Trace*)**.** *Let $E \in \mathcal{E}_h$ and $\mathbf{v} \in \mathbf{V}_h$.*

(i) For any $W \in CW_0^2(E)$, there holds

$$(\nabla_w \mathbf{v}, W)_E = \langle \mathbf{v}^\partial - tr(\mathbf{v}^\circ), W\mathbf{n}\rangle_{E^\partial}. \tag{24}$$

(ii) For any $w \in P_0(E)$, there holds

$$(\nabla_w \cdot \mathbf{v}, w)_E = \langle \mathbf{v}^\partial - tr(\mathbf{v}^\circ), w\mathbf{n}\rangle_{E^\partial}. \tag{25}$$

Proof. For item (i), we apply the definition of discrete weak gradient to obtain

$$(\nabla_w \mathbf{v}, W)_E = \langle \mathbf{v}^\partial, W\mathbf{n}\rangle_{E^\partial} - (\mathbf{v}^\circ, \nabla \cdot W)_{E^\circ}.$$

For $(\mathbf{v}^\circ, \nabla \cdot W)_{E^\circ}$, integration by parts, Gauss Divergence Theorem, and the fact that $\nabla \mathbf{v}^\circ = 0$ (the usual gradient of a constant vector is a zero matrix) all combined lead us to

$$(\mathbf{v}^\circ, \nabla \cdot W)_{E^\circ} = \langle \mathrm{tr}(\mathbf{v}^\circ), W\mathbf{n}\rangle_{E^\partial} - (\nabla \mathbf{v}^\circ, W)_{E^\circ} = \langle \mathrm{tr}(\mathbf{v}^\circ), W\mathbf{n}\rangle_{E^\partial}.$$

Combining the above equalities gives the desired one in (i). Similar ideas produce a proof for item (ii). □

Lemma 3 (*Trace Equivalence for CW_0^2*)**.** *Let E be a polygon. There holds*

$$\|W\mathbf{n}\|_{E^\partial}^2 \approx h_E^{-1}\|W\|_E^2, \qquad \forall W \in CW_0^2(E). \tag{26}$$

Proof. In [8], we established a similar equivalence relationship for vector-valued functions in $CW_0(E)$, which can now be utilized to prove (26). □

Lemma 4 (*A Relationship between the Two Semi-norms*)**.** *There holds*

$$|\,\|\mathbf{v}\|\,|_h \lesssim |\,\|\mathbf{v}\|\,|_1, \qquad \forall \mathbf{v} \in \mathbf{V}_h. \tag{27}$$

Proof. Let $\mathbf{v} \in \mathbf{V}_h$. Consider a convex polygon E with n vertices. Note that $\dim(CW_0^2(E)) = 2n$ and $\mathbf{v}^\partial$ offers $2n$ constant vectors on all n edges together. By Section 3 Lemma 0(ii), there exists a $W \in CW_0^2(E)$ such that

$$(W\mathbf{n})|_{E^\partial} = \mathbf{v}^\partial - \mathrm{tr}(\mathbf{v}^\circ). \tag{28}$$

For this W, applying Lemma 2(i) yields

$$(\nabla_w \mathbf{v}, W)_E = \|\mathbf{v}^\partial - \mathrm{tr}(\mathbf{v}^\circ)\|_{E^\partial}^2. \tag{29}$$

By the Cauchy–Schwarz and Young's inequalities, we have, for any $\delta > 0$,

$$\|\mathbf{v}^\partial - \mathrm{tr}(\mathbf{v}^\circ)\|_{E^\partial}^2 \le \|\nabla_w \mathbf{v}\|_E \|W\|_E \le \frac{1}{2\delta}\|\nabla_w \mathbf{v}\|_E^2 + \frac{\delta}{2}\|W\|_E^2. \tag{30}$$

By Lemma 3, there exists an absolute constant C such that

$$\|W\|_E^2 \le Ch_E\|W\mathbf{n}\|_{E^\partial}^2. \tag{31}$$

So we have

$$\|\mathbf{v}^\partial - \mathrm{tr}(\mathbf{v}^\circ)\|_{E^\partial}^2 \le \frac{1}{2\delta}\|\nabla_w \mathbf{v}\|_E^2 + \frac{\delta}{2}Ch_E\|\mathbf{v}^\partial - \mathrm{tr}(\mathbf{v}^\circ)\|_{E^\partial}^2. \tag{32}$$

Rearranging the terms yields

$$2\delta\left(1 - \frac{\delta}{2}Ch_E\right)\|\mathbf{v}^\partial - \mathrm{tr}(\mathbf{v}^\circ)\|_{E^\partial}^2 \le \|\nabla_w \mathbf{v}\|_E^2. \tag{33}$$

By choosing $\delta = 1/(Ch_E)$, we obtain

$$C^{-1}h_E^{-1}\|\mathbf{v}^\partial - \mathrm{tr}(\mathbf{v}^\circ)\|_{E^\partial}^2 \le \|\nabla_w \mathbf{v}\|_E^2. \tag{34}$$

Summing the above estimate over the entire mesh yields the desired result. □

Lemma 5. *Let $E \in \mathcal{E}_h$ and $\mathbf{v} \in \mathbf{V}_h$. There holds*

$$\|\nabla_w \mathbf{v}\|_E^2 \lesssim h_E^{-1}\|\mathbf{v}^\partial - tr(\mathbf{v}^\circ)\|_{E^\partial}^2, \tag{35}$$

$$\|\nabla_w \cdot \mathbf{v}\|_E^2 \lesssim h_E^{-1}\|\mathbf{v}^\partial - tr(\mathbf{v}^\circ)\|_{E^\partial}^2. \tag{36}$$

Proof. The first inequality can be proved using the same techniques employed in the proof for [8] Lemma 5. Once gain, mesh shape-regularity, in particular, $|E|/|E^\partial| \approx h_E$, is used. The second inequality can be proved similarly. □

Lemma 6 (*More about Semi-norms*). *The two semi-norms* $|\|\cdot\|\|_1$ *and* $|\|\cdot\|\|_h$ *are equivalent on* $\mathbf{V}_h$. *They both become norms on* $\mathbf{V}_h^0$.

Proof. The first statement is obtained by combining Lemmas 4 and 5. We just need to prove the second one.

Consider $\mathbf{v} \in \mathbf{V}_h^0$ such that $|\|\mathbf{v}\|\|_h = 0$. Then $\|\mathbf{v}^\partial - \mathrm{tr}(\mathbf{v}^\circ)\|_{E^\partial}^2 = 0$ for each polygon E in the mesh. Since $\mathbf{v}^\circ = \mathbf{0}$ on the boundary edges, this implies that $\mathbf{v}^\circ = \mathbf{v}^\partial = \mathbf{0}$ for all polygon interiors and all edges. □

5.2. Error equation

Assume $(\mathbf{u}, p)$ are the exact solutions of the Stokes problem (1). We define two linear functionals for $\mathbf{v} \in \mathbf{V}_h$ by

$$\mathcal{G}_1(\mathbf{u}, \mathbf{v}) = \sum_{E\in\mathcal{E}_h} \langle (\mathbb{Q}_h(\nabla\mathbf{u}) - \nabla\mathbf{u})\mathbf{n},\ \mathbf{v}^\partial - \mathrm{tr}(\mathbf{v}^\circ)\rangle_{E^\partial}, \tag{37}$$

$$\mathcal{G}_2(p, \mathbf{v}) = -\sum_{E\in\mathcal{E}_h} \langle (Q_h p - p)\mathbf{n},\ \mathbf{v}^\partial - \mathrm{tr}(\mathbf{v}^\circ)\rangle_{E^\partial}. \tag{38}$$

We also define two discrete errors:

$$\mathbf{e}_h = \{\mathbf{e}_h^\circ, \mathbf{e}_h^\partial\} = \mathbf{Q}_h\mathbf{u} - \mathbf{u}_h, \qquad e_h = Q_h p - p_h. \tag{39}$$

Lemma 7 (*Error Equation*). *Let* $(\mathbf{u}, p)$ *be the exact solutions of* (1) *and* $(\mathbf{u}_h, p_h)$ *be the numerical solutions obtained from* (21). *Let* $\mathbf{e}_h$ *and* e_h *be the errors defined above. For any* $\mathbf{v} \in \mathbf{V}_h^0$, $q \in W_h$ *the following hold*

$$\begin{cases} \mathcal{A}_h(\mathbf{e}_h, \mathbf{v}) - \mathcal{B}_h(e_h, \mathbf{v}) &= \mathcal{G}_1(\mathbf{u}, \mathbf{v}) + \mathcal{G}_2(p, \mathbf{v}), \\ \mathcal{B}_h(q, \mathbf{e}_h) &= 0, \end{cases} \tag{40}$$

where $\mathcal{G}_1, \mathcal{G}_2$ *are defined in* (37) and (38).

Proof. For simplicity, we assume $\mu = 1$. Testing the first PDE in (1) by $\mathbf{v} = \{\mathbf{v}^\circ, \mathbf{v}^\partial\} \in \mathbf{V}_h^0$ on each polygonal element $E \in \mathcal{E}_h$, we obtain

$$(\mathbf{f}, \mathbf{v}^\circ)_E = (-\nabla\cdot\nabla\mathbf{u}, \mathbf{v}^\circ)_E + (\nabla p, \mathbf{v}^\circ)_E. \tag{41}$$

For the 1st term on the right side, we apply integration by parts to get

$$(-\nabla\cdot\nabla\mathbf{u}, \mathbf{v}^\circ)_E = (\nabla\mathbf{u}, \nabla\mathbf{v}^\circ)_E - \langle (\nabla\mathbf{u})\mathbf{n},\ \mathrm{tr}(\mathbf{v}^\circ)\rangle_{E^\partial}. \tag{42}$$

For the 2nd term, we have

$$(\nabla p, \mathbf{v}^\circ)_E = -(p, \nabla\cdot\mathbf{v}^\circ)_E + \langle p\mathbf{n},\ \mathrm{tr}(\mathbf{v}^\circ)\rangle_{E^\partial}. \tag{43}$$

We note the following facts:

(i) $\mathbf{v}^\circ$ is a constant vector function inside each polygon E, so $\nabla\mathbf{v}^\circ = 0$ (zero matrix) and $\nabla\cdot\mathbf{v}^\circ = 0$ (zero scalar) on E;
(ii) the exact solutions $(\mathbf{u}, p)$ have normal continuity across the interior edges;
(iii) $\mathbf{v}^\partial = \mathbf{0}$ on boundary edges.

Summing the above two equalities over the entire mesh and applying the above facts, we obtain

$$\begin{aligned} \sum_{E\in\mathcal{E}_h} (\mathbf{f}, \mathbf{v}^\circ)_E &= \sum_{E\in\mathcal{E}_h} \langle (\nabla\mathbf{u})\mathbf{n},\ \mathbf{v}^\partial - \mathrm{tr}(\mathbf{v}^\circ)\rangle_{E^\partial} \\ &- \sum_{E\in\mathcal{E}_h} \langle p\mathbf{n},\ \mathbf{v}^\partial - \mathrm{tr}(\mathbf{v}^\circ)\rangle_{E^\partial}. \end{aligned} \tag{44}$$

Then we use the 1st equation in the numerical scheme (21) to get

$$\begin{aligned} \mathcal{A}_h(\mathbf{u}_h, \mathbf{v}) - \mathcal{B}_h(p_h, \mathbf{v}) &= \sum_{E\in\mathcal{E}_h} \langle (\nabla\mathbf{u})\mathbf{n},\ \mathbf{v}^\partial - \mathrm{tr}(\mathbf{v}^\circ)\rangle_{E^\partial} \\ &- \sum_{E\in\mathcal{E}_h} \langle p\mathbf{n},\ \mathbf{v}^\partial - \mathrm{tr}(\mathbf{v}^\circ)\rangle_{E^\partial}. \end{aligned} \tag{45}$$

On the other hand, applying Lemmas 1 and 2(i), we arrive at

$$\begin{aligned}\mathcal{A}_h(\mathbf{Q}_h\mathbf{u},\mathbf{v}) &= \sum_{E\in\mathcal{E}_h}(\nabla_w(\mathbf{Q}_h\mathbf{u}),\nabla_w\mathbf{v})_E\\ &= \sum_{E\in\mathcal{E}_h}(\mathbb{Q}_h(\nabla\mathbf{u}),\nabla_w\mathbf{v})_E\\ &= \sum_{E\in\mathcal{E}_h}\langle(\mathbb{Q}_h\nabla\mathbf{u})\mathbf{n},\ \mathbf{v}^\partial-\mathrm{tr}(\mathbf{v}^\circ)\rangle_{E^\partial}\end{aligned} \tag{46}$$

and similarly by Lemmas 1 and 2(ii),

$$\begin{aligned}\mathcal{B}_h(Q_hp,\mathbf{v}) &= \sum_{E\in\mathcal{E}_h}(Q_hp,\nabla_{w,d}\cdot\mathbf{v})_E\\ &= \sum_{E\in\mathcal{E}_h}\langle(Q_hp)\mathbf{n},\mathbf{v}^\partial-\mathrm{tr}(\mathbf{v}^\circ)\rangle_{E^\partial}.\end{aligned} \tag{47}$$

Combining the above two formulas gives

$$\begin{aligned}\mathcal{A}_h(\mathbf{Q}_h\mathbf{u},\mathbf{v})-\mathcal{B}_h(Q_hp,\mathbf{v}) &= \sum_{E\in\mathcal{E}_h}\langle(\mathbb{Q}_h(\nabla\mathbf{u}))\mathbf{n},\ \mathbf{v}^\partial-\mathrm{tr}(\mathbf{v}^\circ)\rangle_{E^\partial}\\ &- \sum_{E\in\mathcal{E}_h}\langle(Q_hp)\mathbf{n},\ \mathbf{v}^\partial-\mathrm{tr}(\mathbf{v}^\circ)\rangle_{E^\partial}.\end{aligned} \tag{48}$$

Subtracting (45) from (48) yields

$$\mathcal{A}_h(\mathbf{e}_h,\mathbf{v})-\mathcal{B}_h(e_h,\mathbf{v})=\mathcal{G}_1(\mathbf{u},\mathbf{v})+\mathcal{G}_2(p,\mathbf{v}). \tag{49}$$

Again, for each polygonal element E, applying Lemma 1(ii) along with the incompressibility $\nabla\cdot\mathbf{u}=0$ gives

$$(q,\nabla_w\cdot(\mathbf{Q}_h\mathbf{u}))_E=(q,Q_h(\nabla\cdot\mathbf{u}))_E=0. \tag{50}$$

Then we have

$$(q,\nabla_w\cdot\mathbf{e}_h)_E=(q,\nabla_w\cdot(\mathbf{Q}_h\mathbf{u}-\mathbf{u}_h))_E=-(q,\nabla_w\cdot\mathbf{u}_h)_E. \tag{51}$$

Summing the above equality over the entire mesh gives

$$\mathcal{B}_h(q,\mathbf{e}_h)=-\mathcal{B}_h(q,\mathbf{u}_h)=0, \tag{52}$$

where we have used the 2nd equation in the numerical scheme (21). □

Lemma 8. *There exists a constant $C>0$ independent of h such that*

$$\sup_{\mathbf{v}\in\mathbf{V}_h^0}\frac{(\nabla_w\cdot\mathbf{v},q)}{|\,\|\mathbf{v}\|\,|_h}\geq C\|q\|,\qquad\forall q\in W_h. \tag{53}$$

Proof. For $\forall q\in W_h$, it is known that there exists $\tilde{\mathbf{v}}\in H_0^1(\Omega)^2$ such that

$$\frac{(\nabla\cdot\tilde{\mathbf{v}},q)}{\|\nabla\tilde{\mathbf{v}}\|}\geq C\|q\|. \tag{54}$$

Let $\mathbf{v}=\mathbf{Q}_h\tilde{\mathbf{v}}$. By Lemma 1(i), we have (elementwise and then meshwise)

$$\|\nabla_w\mathbf{v}\|=\|\nabla_w(\mathbf{Q}_h\tilde{\mathbf{v}})\|=\|\mathbb{Q}_h(\nabla\tilde{\mathbf{v}})\|\leq\|\nabla\tilde{\mathbf{v}}\|. \tag{55}$$

Using Lemma 1(ii) together with the definition of Q_h, we have

$$(\nabla_w\cdot\mathbf{v},q)=(\nabla_w\cdot(\mathbf{Q}_h\tilde{\mathbf{v}}),q)=(Q_h(\nabla\cdot\tilde{\mathbf{v}}),q)=(\nabla\cdot\tilde{\mathbf{v}},q). \tag{56}$$

Combining (54), (55), (56), and the semi-norm equivalence, we have

$$\frac{(\nabla_w\cdot\mathbf{v},q)}{|\,\|\mathbf{v}\|\,|_h}\geq\frac{(\nabla_w\cdot\mathbf{v},q)}{\|\nabla_w\mathbf{v}\|}\geq\frac{(\nabla\cdot\tilde{\mathbf{v}},q)}{\|\nabla\tilde{\mathbf{v}}\|}\geq C\|q\|, \tag{57}$$

which completes the proof. □

5.3. Energy norm error estimate

For any function $\psi\in H^1(E)$, the following trace inequality holds true

$$\|\psi\|_{E^\partial}^2\leq C(h_E^{-1}\|\psi\|_{E^\circ}^2+h_E\|\nabla\psi\|_{E^\circ}^2). \tag{58}$$

Theorem 1 (*1st Order Convergence in Energy Norm*). *Let* $(\mathbf{u}, p)$ *be the exact solutions of* (1) *and* $(\mathbf{u}_h, p_h)$ *be the numerical solutions of* (21). *Then*

$$| \|\mathbf{Q}_h\mathbf{u} - \mathbf{u}_h\| |_1 \leq Ch(\|\mathbf{u}\|_2 + \|p\|_1), \tag{59}$$

$$\|Q_h p - p_h\| \leq Ch(\|\mathbf{u}\|_2 + \|p\|_1). \tag{60}$$

Proof. Let $\mathbf{v} = \mathbf{e}_h$ and $q = e_h$ in (40). Adding those two equations yields

$$| \|\mathbf{e}_h| \|_1^2 = \mathcal{A}_h(\mathbf{e}_h, \mathbf{e}_h) = \mathcal{G}_1(\mathbf{u}, \mathbf{e}_h) + \mathcal{G}_2(p, e_h). \tag{61}$$

By the Cauchy–Schwarz inequality, the trace inequality, the approximation capacity of $\mathbb{Q}_h$, the definition of semi-norm $| \|\cdot\| |_h$, and the shape regularity of the polygonal mesh, we have

$$\begin{aligned} |\mathcal{G}_1(\mathbf{u}, \mathbf{e}_h)| &= \Big| \sum_{E\in\mathcal{E}_h} \langle (\mathbb{Q}_h(\nabla\mathbf{u}) - \nabla\mathbf{u})\mathbf{n},\ \mathbf{e}_h^\partial - \mathrm{tr}(\mathbf{e}_h^\circ)\rangle_{E^\partial} \Big| \\ &\leq \left(\sum_{E\in\mathcal{E}_h} h_E \|\mathbb{Q}_h(\nabla\mathbf{u}) - \nabla\mathbf{u}\|_{E^\partial}^2 \right)^{\frac{1}{2}} \left(\sum_{E\in\mathcal{E}_h} h_E^{-1} \|\mathbf{e}_h^\partial - \mathrm{tr}(\mathbf{e}_h^\circ)\|_{E^\partial}^2 \right)^{\frac{1}{2}} \\ &\leq Ch\|\mathbf{u}\|_2 | \|\mathbf{e}_h\| |_h. \end{aligned} \tag{62}$$

Similarly, we have

$$\begin{aligned} |\mathcal{G}_2(p, \mathbf{e}_h)| &= \Big| -\sum_{E\in\mathcal{E}_h} \langle (Q_h p - p)\mathbf{n},\ \mathbf{e}_h^\partial - \mathrm{tr}(\mathbf{e}_h^\circ)\rangle_{E^\partial} \Big| \\ &\leq \left(\sum_{E\in\mathcal{E}_h} h_E \|Q_h p - p\|_{E^\partial}^2 \right)^{\frac{1}{2}} \left(\sum_{E\in\mathcal{E}_h} h_E^{-1} \|\mathbf{e}_h^\partial - \mathrm{tr}(\mathbf{e}_h^\circ)\|_{E^\partial}^2 \right)^{\frac{1}{2}} \\ &\leq Ch\|p\|_1 | \|\mathbf{e}_h| \|_h. \end{aligned} \tag{63}$$

Combining the estimates in (62) and (63) and applying the equivalence between $| \|\cdot\| |_1$ and $| \|\cdot\| |_h$, we obtain

$$| \|\mathbf{e}_h| \|_1 \leq Ch(\|\mathbf{u}\|_2 + \|p\|_1). \tag{64}$$

The above estimation applies to any $\mathbf{v} \in \mathbf{V}_h^0$ as well and hence yields

$$|\mathcal{G}_1(\mathbf{u}, \mathbf{v}) + \mathcal{G}_2(p, \mathbf{v})| \leq Ch(\|\mathbf{u}\|_2 + \|p\|_1) | \|\mathbf{v}\| |_h. \tag{65}$$

Applying the Cauchy–Schwarz inequality and the semi-norm equivalence yields

$$|\mathcal{A}_h(\mathbf{e}_h, \mathbf{v})| \leq C | \|\mathbf{e}_h| \|_1 | \|\mathbf{v}\| |_1 \leq C | \|\mathbf{e}_h| \|_1 | \|\mathbf{v}\| |_h. \tag{66}$$

Using (40), we obtain

$$\begin{aligned} |\mathcal{B}_h(e_h, \mathbf{v})| &= |\mathcal{A}_h(\mathbf{e}_h, \mathbf{v}) - \mathcal{G}_1(\mathbf{u}, \mathbf{v}) - \mathcal{G}_2(p, \mathbf{v})| \\ &\leq Ch(\|\mathbf{u}\|_2 + \|p\|_1) | \|\mathbf{v}\| |_h. \end{aligned} \tag{67}$$

The above estimate together with Lemma 8 implies

$$\|e_h\| \leq Ch(\|\mathbf{u}\|_2 + \|p\|_1), \tag{68}$$

which concludes the proof. □

5.4. L^2-norm error estimate for velocity

In this section, we derive an L^2-norm error estimate for velocity based on a duality argument. To this end, we consider the following dual problem

$$\begin{cases} -\Delta\Phi + \nabla\xi = \mathbf{e}_h^\circ & \text{in } \Omega, \\ \nabla\cdot\Phi = 0 & \text{in } \Omega, \\ \Phi = \mathbf{0}, & \text{on } \partial\Omega, \end{cases} \tag{69}$$

for which the dual solutions are assumed to have full regularity $(\Phi, \xi) \in H_0^2(\Omega)^d \times H^1(\Omega)$ along with

$$\|\Phi\|_2 + \|\xi\|_1 \leq C\|\mathbf{e}_h^\circ\|. \tag{70}$$

Theorem 2 (L^2*-norm Error Estimate for Velocity*)**.** *Let* $(\mathbf{u}, p)$ *be the exact solutions of* (1) *and* $(\mathbf{u}_h, p_h)$ *be the numerical solutions obtained from* (21)*. Assume additionally* $\mathbf{f} \in H^1(\Omega)^2$*. Then*

$$\|\mathbf{Q}_h^\circ \mathbf{u} - \mathbf{u}_h^\circ\| \leq Ch^2(\|\mathbf{u}\|_2 + \|p\|_1 + \|\mathbf{f}\|_1). \tag{71}$$

Therefore, after combining with the projection error, we have

$$\|\mathbf{u} - \mathbf{u}_h^\circ\| \leq Ch(\|\mathbf{u}\|_2 + \|p\|_1 + \|\mathbf{f}\|_1). \tag{72}$$

Proof. Consider a polygonal element $E \in \mathcal{E}_h$. We test the 1st equation in the dual problem (69) by $\mathbf{e}_h^\circ$ to obtain

$$(-\nabla \cdot \nabla \Phi, \mathbf{e}_h^\circ)_{E^\circ} + (\nabla \xi, \mathbf{e}_h^\circ)_{E^\circ} = (\mathbf{e}_h^\circ, \mathbf{e}_h^\circ)_{E^\circ}. \tag{73}$$

For the first term on the left side of (73), we apply the definition of discrete weak gradient to obtain

$$(-\nabla \cdot \nabla \Phi, \mathbf{e}_h^\circ)_{E^\circ} = (\nabla \Phi, \nabla_w \mathbf{e}_h)_E - \langle (\nabla \Phi)\mathbf{n}, \mathbf{e}_h^\partial \rangle_{E^\partial}. \tag{74}$$

Summing the above equality over the mesh along with application of the normal continuity of $\nabla \Phi$ and the definition of $\mathbb{Q}_h$, we obtain

$$\begin{aligned} \sum_{E\in\mathcal{E}_h} (-\nabla \cdot \nabla \Phi, \mathbf{e}_h^\circ)_{E^\circ} &= \sum_{E\in\mathcal{E}_h} (\nabla \Phi, \nabla_w \mathbf{e}_h)_E \\ &= \sum_{E\in\mathcal{E}_h} (\mathbb{Q}_h(\nabla \Phi), \nabla_w \mathbf{e}_h)_E. \\ &= \sum_{E\in\mathcal{E}_h} (\mathbb{Q}_h(\nabla \Phi) - \nabla \Phi, \nabla_w \mathbf{e}_h)_E + \sum_{E\in\mathcal{E}_h} (\nabla \Phi, \nabla_w \mathbf{e}_h)_E. \end{aligned} \tag{75}$$

The 1st term on the right side of (75) can be estimated utilizing the Cauchy–Schwarz inequality, the approximation capacity of $\mathbb{Q}_h$, the regularity of Φ, and Theorem 1:

$$\left| \sum_{E\in\mathcal{E}_h} (\mathbb{Q}_h(\nabla \Phi) - \nabla \Phi, \nabla_w \mathbf{e}_h)_E \right| \leq Ch^2(\|\mathbf{u}\|_2 + \|p\|_1)\|\Phi\|_2. \tag{76}$$

For the 2nd term on the right side of (75), applying the definition of $\mathbf{e}_h$, Lemma 1(i), the definition of $\mathbb{Q}_h$, and the orthogonality induced by $\mathbb{Q}_h$, we have

$$\begin{aligned} (\nabla \Phi, \nabla_w \mathbf{e}_h)_E &= (\nabla \Phi, \nabla_w(\mathbf{Q}_h \mathbf{u}))_E - (\nabla \Phi, \nabla_w \mathbf{u}_h)_E \\ &= (\nabla \Phi, \mathbb{Q}_h(\nabla \mathbf{u}))_E - (\nabla \Phi, \nabla_w \mathbf{u}_h)_E \\ &= (\nabla \Phi, \mathbb{Q}_h(\nabla \mathbf{u}))_E - (\mathbb{Q}_h(\nabla \Phi), \nabla_w \mathbf{u}_h)_E \\ &= (\nabla \Phi, \mathbb{Q}_h(\nabla \mathbf{u}))_E - (\nabla_w(\mathbf{Q}_h \Phi), \nabla_w \mathbf{u}_h)_E \\ &= (\nabla \Phi, \mathbb{Q}_h(\nabla \mathbf{u}) - \nabla \mathbf{u})_E + (\nabla \Phi, \nabla \mathbf{u})_E - (\nabla_w(\mathbf{Q}_h \Phi), \nabla_w \mathbf{u}_h)_E \\ &= (\nabla \Phi - \mathbb{Q}_h(\nabla \Phi), \mathbb{Q}_h(\nabla \mathbf{u}) - \nabla \mathbf{u})_E \\ &\quad + (\nabla \Phi, \nabla \mathbf{u})_E - (\nabla_w(\mathbf{Q}_h \Phi), \nabla_w \mathbf{u}_h)_E. \end{aligned} \tag{77}$$

Summing the above result over the mesh gives

$$\begin{aligned} \sum_{E\in\mathcal{E}_h} (\nabla \Phi, \nabla_w \mathbf{e}_h)_E &= \sum_{E\in\mathcal{E}_h} (\nabla \Phi - \mathbb{Q}_h(\nabla \Phi), \mathbb{Q}_h(\nabla \mathbf{u}) - \nabla \mathbf{u})_E \\ &\quad + \sum_{E\in\mathcal{E}_h} (\nabla \Phi, \nabla \mathbf{u})_E - \sum_{E\in\mathcal{E}_h} (\nabla_w(\mathbf{Q}_h \Phi), \nabla_w \mathbf{u}_h)_E. \end{aligned} \tag{78}$$

Testing the first PDE in the Stokes problem (1) by Φ and applying the normal continuity of $\nabla \mathbf{u}$ and also the fact that $\nabla \cdot \Phi = 0$, we obtain

$$\sum_{E\in\mathcal{E}_h} (\nabla \mathbf{u}, \nabla \Phi)_E = \sum_{E\in\mathcal{E}_h} (\mathbf{f}, \nabla \Phi). \tag{79}$$

On the other hand, we take $\mathbf{v} = \mathbf{Q}_h \Phi$ in the 1st equation of Scheme I and then apply the fact that $\nabla_w(\mathbf{Q}_h \Phi) = Q_h(\nabla \cdot \Phi) = 0$ to get

$$\sum_{E\in\mathcal{E}_h} (\nabla_w \mathbf{u}_h, \nabla_w(\mathbf{Q}_h \Phi))_E = \sum_{E\in\mathcal{E}_h} (\mathbf{f}, \mathbf{Q}_h^\circ \Phi)_E. \tag{80}$$

Together, these lead to

$$\begin{aligned}&\sum_{E\in\mathcal{E}_h}(\nabla\mathbf{\Phi},\nabla\mathbf{u})_E-\sum_{E\in\mathcal{E}_h}(\nabla_w(\mathbf{Q}_h\mathbf{\Phi}),\nabla_w\mathbf{u}_h)_E\\&=\sum_{E\in\mathcal{E}_h}(\mathbf{f},\mathbf{\Phi}-\mathbf{Q}_h^\circ\mathbf{\Phi})_E=\sum_{E\in\mathcal{E}_h}(\mathbf{f}-\mathbf{Q}_h^\circ\mathbf{f},\mathbf{\Phi}-\mathbf{Q}_h^\circ\mathbf{\Phi})_E,\end{aligned}\tag{81}$$

where we have used the orthogonality induced by $\mathbf{Q}_h^\circ$.

Combining the results in (81) and (78), we arrive at

$$\begin{aligned}\sum_{E\in\mathcal{E}_h}(\nabla\mathbf{\Phi},\nabla_w\mathbf{e}_h)_E&=\sum_{E\in\mathcal{E}_h}(\nabla\mathbf{\Phi}-\mathbb{Q}_h(\nabla\mathbf{\Phi}),\mathbb{Q}_h(\nabla\mathbf{u})-\nabla\mathbf{u})_E\\&+\sum_{E\in\mathcal{E}_h}(\mathbf{f}-\mathbf{Q}_h^\circ\mathbf{f},\mathbf{\Phi}-\mathbf{Q}_h^\circ\mathbf{\Phi})_E.\end{aligned}\tag{82}$$

Applying the approximation properties of $\mathbb{Q}_h$ and $\mathbf{Q}_h^\circ$ along with the regularity assumption on $\mathbf{u}$, $\mathbf{\Phi}$, $\mathbf{f}$, we arrive at

$$\left|\sum_{E\in\mathcal{E}_h}(\nabla\mathbf{\Phi},\nabla_w\mathbf{e}_h)_E\right|\le Ch^2(\|\mathbf{u}\|_2+\|\mathbf{f}\|_1)\|\mathbf{\Phi}\|_2.\tag{83}$$

Combining the estimates in (83), (76), and (75), we obtain

$$\left|\sum_{E\in\mathcal{E}_h}(-\nabla\cdot\nabla\mathbf{\Phi},\mathbf{e}_h^\circ)_{E^\circ}\right|\le Ch^2(\|\mathbf{u}\|_2+\|p\|_1+\|\mathbf{f}\|_1).\tag{84}$$

Now we go back to estimate the second term on the left side of (73). Applying integration by parts, the definition of Q_h, the definition of discrete weak divergence, we have

$$\begin{aligned}(\nabla\xi,\mathbf{e}_h^\circ)_{E^\circ}&=-(\xi,\nabla\cdot\mathbf{e}_h^\circ)_{E^\circ}+\langle\xi\mathbf{n},\mathrm{tr}(\mathbf{e}_h^\circ)\rangle_{E^\partial}\\&=-(Q_h\xi,\nabla\cdot\mathbf{e}_h^\circ)_{E^\circ}+\langle\xi\mathbf{n},\mathrm{tr}(\mathbf{e}_h^\circ)\rangle_{E^\partial}\\&=(\nabla(Q_h\xi),\mathbf{e}_h^\circ)_{E^\circ}-\langle(Q_h\xi)\mathbf{n},\mathrm{tr}(\mathbf{e}_h^\circ)\rangle_{E^\partial}+\langle\xi\mathbf{n},\mathrm{tr}(\mathbf{e}_h^\circ)\rangle_{E^\partial}\\&=-(Q_h\xi,\nabla_w\cdot\mathbf{e}_h)_E+\langle(Q_h\xi)\mathbf{n},\mathbf{e}_h^\partial\rangle_{E^\partial}\\&\quad-\langle(Q_h\xi)\mathbf{n},\mathrm{tr}(\mathbf{e}_h^\circ)\rangle_{E^\partial}+\langle\xi\mathbf{n},\mathrm{tr}(\mathbf{e}_h^\circ)\rangle_{E^\partial}.\end{aligned}\tag{85}$$

Summing the above result over the mesh, applying the definition of $\mathcal{B}_h$ and then the fact that $\mathcal{B}_h(Q_h\xi,\mathbf{e}_h)=0$, along with the normal continuity of ξ, we obtain

$$\sum_{E\in\mathcal{E}_h}(\nabla\xi,\mathbf{e}_h^\circ)_{E^\circ}=\sum_{E\in\mathcal{E}_h}\langle(Q_h\xi-\xi)\mathbf{n},\mathbf{e}_h^\partial-\mathrm{tr}(\mathbf{e}_h^\circ)\rangle_{E^\partial}.\tag{86}$$

This can be estimated similarly as to (63) to end up with

$$\left|\sum_{E\in\mathcal{E}_h}(\nabla\xi,\mathbf{e}_h^\circ)_{E^\circ}\right|\le Ch^2(\|\mathbf{u}\|_2+\|p\|_1)\|\xi\|_1.\tag{87}$$

Combining the estimates in (87) and (84), Eq. (73), along with the dual regularity, we finally obtain

$$\|\mathbf{Q}_h^\circ\mathbf{u}-\mathbf{u}_h^\circ\|=\|\mathbf{e}_h^\circ\|\le Ch^2(\|\mathbf{u}\|_2+\|p\|_1+\|\mathbf{f}\|_1),\tag{88}$$

which completes the proof. □

6. Reduced scheme for the discretely divergence-free subspace and pressure recovery

Note that for the full scheme in (21), the resulting discrete linear system has a size (3#elements + 2#edges). It is a typical saddle-point problem that requires specially designed linear solvers. In this section, we consider a reduction to the discretely divergence-free subspace for velocity and subsequently a procedure for pressure recovery.

6.1. Scheme for velocity in the discretely divergence-free subspace

Let us examine a typical choice of basis functions for the full scheme in (21).

- For each element E, one can choose two discrete weak functions $\mathbf{v}_{E,1}$, $\mathbf{v}_{E,2}$ such that

  $$\mathbf{v}_{E,1}^\circ=[1,0]^T,\qquad\mathbf{v}_{E,2}^\circ=[0,1]^T$$

  inside this element E but be the zero vector inside any other element. Of course, one sets $\mathbf{v}_{E,i}^\partial=\mathbf{0}(i=1,2)$ for any edge in the mesh. The definition of discrete weak divergence in (17) implies that

  $$\nabla_w\cdot(\mathbf{v}_{E,1})=0,\qquad\nabla_w\cdot(\mathbf{v}_{E,2})=0$$

  on any element in the mesh.

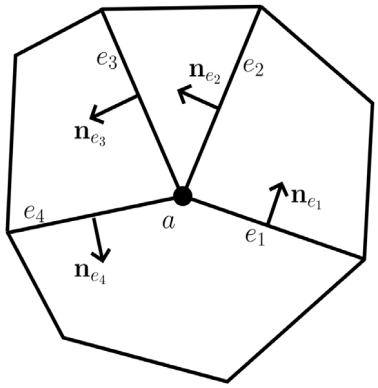

Fig. 1. A node-based basis function for the discretely divergence-free subspace.

- For each edge e in the mesh, one can choose a discrete weak function

$$\mathbf{v} = \{\mathbf{v}^\circ, \mathbf{v}^\partial\} = \{\mathbf{0}, \mathbf{t}_e\}.$$

  Again it can be easily shown that $\nabla_w \cdot \mathbf{v} = 0$ on any element in the mesh.
- For each edge e in the mesh, if one chooses a discrete weak function

$$\mathbf{v} = \{\mathbf{v}^\circ, \mathbf{v}^\partial\} = \{\mathbf{0}, \mathbf{n}_e\},$$

  then for any element E that has e as a part of its boundary, there holds

$$(\nabla_w \cdot \mathbf{v})|_E = \frac{|e|}{|E|}(\mathbf{n}_e \cdot \mathbf{n}_E),$$

  where $\mathbf{n}_E$ is the outward unit normal vector on the boundary of E.

Based on the above analysis, we use three groups of basis functions to span the discretely divergence-free subspace $\mathbf{V}_h^{ddf}$ for velocity.

(i) *Element-based*: For each polygonal element, consider the two local basis functions $[1, 0]^T$, $[0, 1]^T$;
(ii) *Edge-based*: For each edge e, consider the local basis function on the edge that involves only the unit tangential vector $\mathbf{t}_e$.
(iii) *Node-based*: For each interior node a that is connected to edges $e_1, e_2, \ldots, e_m$, assume the unit normal vectors are $\mathbf{n}_{e_1}, \mathbf{n}_{e_2}, \ldots, \mathbf{n}_{e_m}$ and they are oriented counterclockwise (see Fig. 1), we define

$$\mathbf{v}_a = \frac{1}{|e|_1}\mathbf{n}_{e_1} + \cdots + \frac{1}{|e|_m}\mathbf{n}_{e_m}.$$

Then for each polygonal element E participating in the hull made by the other endpoints of these edges, we have

$$(\nabla_w \cdot \mathbf{v}_a)|_E = 0.$$

This is simply because one edge has flow in and the next edge has flow out. This construction extends to boundary nodes also.

It is interesting to notice that the above Type (ii) and (iii) basis functions have some features similar to those edge-midpoint-based basis functions used in [4].

It is also interesting to note that

$$\dim(\mathbf{V}_h) = 2\,\#\text{elements} + 2\,\#\text{edges}, \tag{89}$$

$$\dim(\mathbf{V}_h^{ddf}) = 2\,\#\text{elements} + \#\text{edges} + \#\text{nodes}. \tag{90}$$

We shall have $\dim(\mathbf{V}_h^{ddf}) < \dim(\mathbf{V}_h)$, since #nodes < #edges generally for a polygonal mesh. For example, for a uniform rectangular mesh with n partitions each in the x-, y-directions, there holds

$$\#\text{nodes} = (n+1)^2 < 2n(n+1) = \#\text{edges}.$$

Scheme II. Seek $\mathbf{u}_h^{ddf} \in \mathbf{V}_h^{ddf}$ such that

$$\sum_{E\in\mathcal{E}_h}(\nabla_w \mathbf{u}_h^{ddf}, \nabla_w \mathbf{v})_E = \sum_{E\in\mathcal{E}_h}(\mathbf{f}, \mathbf{v}^\circ)_E, \qquad \forall \mathbf{v} \in \mathbf{V}_h^{ddf}. \tag{91}$$

This results in a symmetric positive-definite linear system that is much easier to be solved than a saddle-point problem.

6.2. Procedure for pressure recovery

Once $\mathbf{u}_h^{ddf} \in \mathbf{V}_h^{ddf}$, namely, the numerical velocity in the discretely divergence-free subspace, is obtained from Scheme II, we use it to recover a numerical pressure p_h, which is a constant on each element.

Note that $\mathbf{u}_h^{ddf}$ still satisfies the first equation in the full scheme (21). To recover a numerical pressure from the aforementioned equation, we shall utilize the test functions $\mathbf{v}$ that are in $\mathbf{V}_h$ but not in $\mathbf{V}_h^{ddf}$. Clearly, we can use the discrete weak functions that take the values of normal vectors on individual edges.

Let Γ_h be the set of all edges in a shape-regular polygonal mesh $\mathcal{E}_h$. Let $e \in \Gamma_h$ and $\mathbf{n}_e$ be a unit normal vector for e. Note that it can be pre-chosen from any of the two possible directions but must be outward to the domain when e is a boundary edge.

Let $\mathbf{v}_e = \{\mathbf{v}^\circ, \mathbf{v}^\partial\}$ be a discrete weak function such that $\mathbf{v}^\partial = \mathbf{n}_e$ only on edge e but be the zero vector on all other edges. In the same spirit, $\mathbf{v}^\circ = \mathbf{0}$ for all element interiors. Let $E \in \mathcal{E}_h$ and $e \subset E^\partial$. Then by the definition of discrete weak divergence in (17), we have

$$(\nabla_w \cdot \mathbf{v}_e)|_E = \frac{|e|}{|E|}(\mathbf{n}_e \cdot \mathbf{n}_E), \tag{92}$$

where $\mathbf{n}_E$ is the unit normal vector on e that is outward to element E. Clearly, $\mathbf{n}_e \cdot \mathbf{n}_E = 1$ if they points to the same direction and -1 otherwise.

Now for the 1st equation of the full scheme (21), we take $\mathbf{v} = \mathbf{v}_e$ for any edge $e \in \Gamma_h$. When e is an interior edge shared by two polygonal elements E_1, E_2, we have

$$|e|\Big((\mathbf{n}_e \cdot \mathbf{n}_{E_1})\, p_h|_{E_1} + (\mathbf{n}_e \cdot \mathbf{n}_{E_2})\, p_h|_{E_2}\Big) = -\mu \sum_{E \in \mathcal{E}_h} (\nabla_w \mathbf{u}_h^{ddf}, \nabla_w \mathbf{v}_e)_E. \tag{93}$$

But the summation on the right side involves only the two elements E_1, E_2 that share e. When e is a boundary edge, only one element is involved.

Conceptually, (93) is a linear system whose number of equations = #edges and whose number of unknowns = #elements. It can be readily solved in `Matlab`. On other platforms, an algorithm can be established by starting with the boundary edges and going over the interior edges to recover the elementwise constant pressure. Then the algorithm would have some features similar to the one in [20].

7. Numerical experiments

This section presents numerical results to illustrate the theoretical analysis in Section 5 and also demonstrates the accuracy and efficiency of our new weak Galerkin finite element solver for Stokes flow.

Example 1 (*A Swirling Velocity with No-slip Boundary Condition*)**.** We consider a problem adopted from [21] that has a swirling velocity with a prescribed pressure:

$$\mathbf{u}(x, y) = (\sin^2(\pi x)\sin(2\pi y), -\sin(2\pi x)\sin^2(\pi y)),$$
$$p(x, y) = \pi \sin(2\pi x)\sin(2\pi y).$$

The domain is the unit square $\Omega = (0, 1)^2$. A no-slip boundary condition ($\mathbf{u} = \mathbf{0}$) is posed on the whole boundary. We set $\mu = 1$ and compute the body force $\mathbf{f}(x, y)$ accordingly.

We test Example 1 on a sequence of polygonal meshes generated by `PolyMesher` [22]. As shown in Fig. 2 left panel, most polygons are pentagons and hexagons, there are few quadrilaterals and 7-gons. Table 1 further reveals the 1st order convergence in numerical velocity obtained by the WG($P_0^2, P_0^2; CW_0^2, P_0$) method.

We test this example also on triangular and rectangular meshes, see Tables 2 and 3, respectively. Again 1st order convergence in velocity and pressure can be clearly observed.

Fig. 2 left panel shows profiles of numerical velocity and pressure obtained from applying the lowest-order WG finite element method (Scheme I) on a level 5 polygonal mesh. The swirling velocity field and the 4 patches of the pressure field are accurately captured by this novel WG method. Fig. 2 right panel shows results from the discretely divergence-free scheme (Scheme II) and the subsequent pressure recovery procedure. The aforementioned flow features are also well captured.

Example 2 (*Lid-driven Cavity*)**.** The lid-driven cavity problem is a popular testcase [13,16,23] that does not have a known exact solution. Let $\Omega = (0, 1)^2$ be the cavity domain and $\mu = 1$. The fluid moves at a unit speed on the upper side, while remaining still on the other three sides. To be more specific, a Dirichlet boundary condition is given as

$$\mathbf{u}|_{\partial\Omega} = \begin{cases} (1, 0) & \text{if } x \in (0, 1), y = 1, \\ (0, 0) & \text{elsewhere.} \end{cases}$$

The boundary condition is discontinuous at the two upper corners, which induces pressure singularity.

Table 1
Example 1 (Swirling velocity): Convergence rates of errors in velocity obtained by lowest-order WG method on polygonal meshes generated by `PolyMesher`.

Lvl.	#Ems	#Egs	h	$\|\|\|\mathbf{Q}_h\mathbf{u}-\mathbf{u}_h\|\|\|_1$	Rate	$\|\mathbf{u}-\mathbf{u}_h^\circ\|_{\mathbf{L}^2}$	Rate
3	64	193	1.8627e−1	5.7257e−1	–	1.5877e−1	–
4	256	769	9.2022e−2	2.8134e−1	1.007	8.0922e−2	0.955
5	1024	3 073	4.5607e−2	1.3837e−1	1.010	3.9715e−2	1.013
6	4096	12 289	2.2752e−2	6.9062e−2	0.999	1.9731e−2	1.005

Table 2
Example 1 (Swirling velocity): 1st order convergence of errors in velocity and pressure obtained by lowest-order WG method on triangular meshes.

Level	#Elements	#Edges	h	$\|\mathbf{u}-\mathbf{u}_h^\circ\|_{\mathbf{L}^2}$	$\|p-p_h\|_{L^2}$
3	128	208	1/8	1.3123e−1	7.3526e−1
4	512	800	1/16	6.5605e−2	3.5999e−1
5	2048	3 136	1/32	3.2751e−2	1.5541e−1
6	8192	12 416	1/64	1.6366e−2	6.8144e−2

Table 3
Example 1: Swirling velocity approximated by the discretely divergence-free scheme on rectangular meshes: 1st order convergence in velocity and recovered pressure.

h	$\|\mathbf{u}-\mathbf{u}_h^\circ\|_{\mathbf{L}^2}$	$\|p-p_h\|_{L^2}$	$p_h^{\min}$	$p_h^{\max}$
1/8	1.6127e−1	7.0427e−1	−2.2908	2.2908
1/16	8.0324e−2	2.8092e−1	−2.9071	2.9071
1/32	4.0102e−2	1.2972e−1	−3.0815	3.0815
1/64	2.0043e−2	6.3438e−2	−3.1265	3.1265

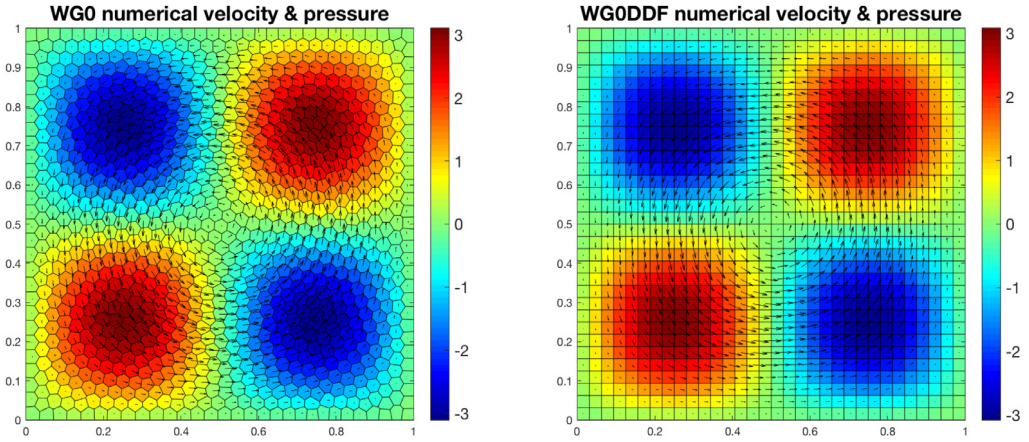

Fig. 2. Example 1 (Swirling velocity): Profiles of numerical velocity and pressure obtained by WG$(P_0^2, P_0^2; CW_0^2, P_0)$ method: *Left*: Scheme I on a polygonal mesh (Level 5); *Right*: Scheme II with pressure recovery on a rectangular mesh ($h = 1/2^5$).

Shown in Fig. 3 are profiles of the numerical velocity and pressure obtained from applying the lowest-order WG method to the lid-driven cavity problem on 8×8 and 16×16 uniform rectangular meshes. Our new WG solver clearly captures the main features of the problem:

- A large eddy located at $(0.5, 0.75)$;
- Pressure singularity (diverging to $\pm\infty$) at the two upper corners.

Example 3 (*Flow Passing a Cylinder*)**.** This benchmark problem has been frequently tested in literature [16,24]. The domain in consideration is $\Omega = (0, 2) \times (0, 1)$ but a cylindrical obstacle with radius 0.1 is placed at $(0.5, 0.5)$. The left- and right-sides of the domain have a prescribed velocity $[1, 0]^T$, whereas the top- and bottom-sides admit a no-slip condition. There is no body force and $\mu = 1$.

Here we test it using our new WG finite element solver on polygonal meshes. Numerical results are presented in Fig. 4. The top panel shows clearly the pressure increase before (on the left of) the obstacle and the pressure drop after (on the

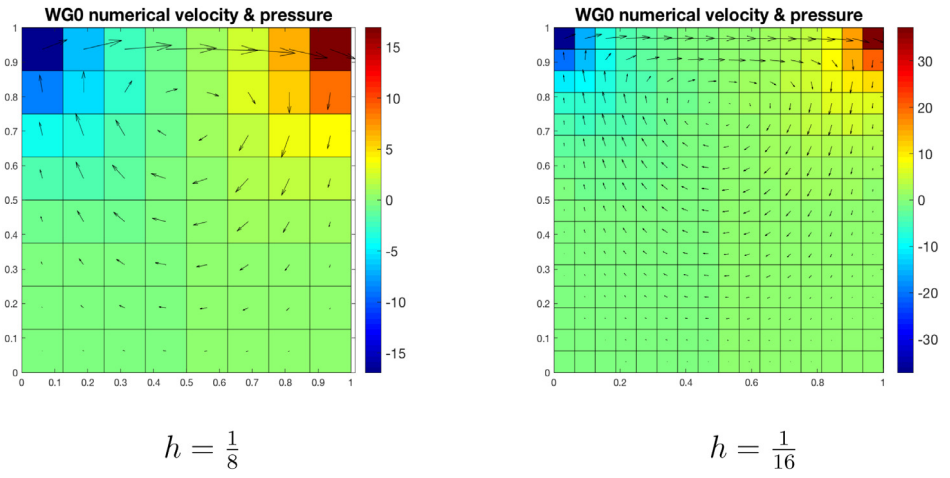

Fig. 3. Example 2 (Lid-driven cavity) simulated by the lowest-order WG method on rectangular meshes. *Left panel*: Numerical velocity and pressure profiles for $h = \frac{1}{8}$; *Right panel*: Numerical velocity and pressure profiles for $h = \frac{1}{16}$.

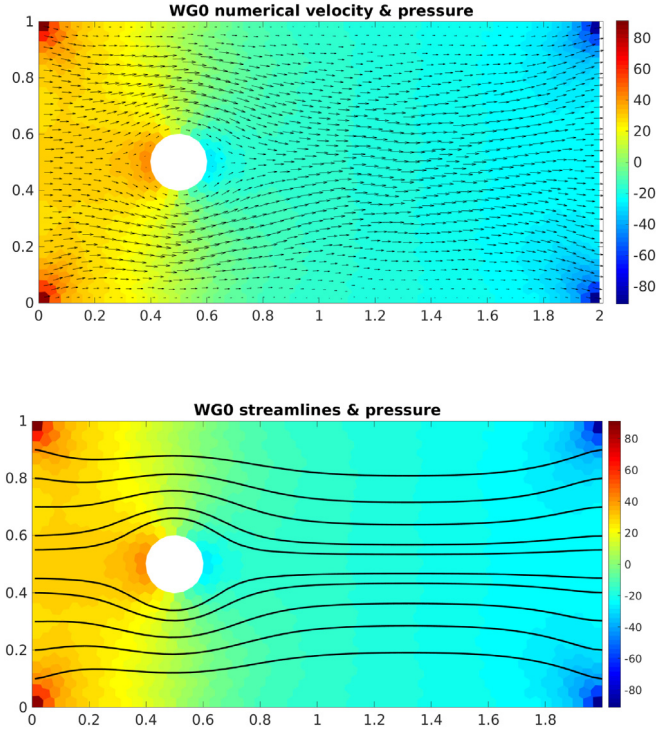

Fig. 4. Example 3 (Flow passing a cylinder) simulated by WG on a polygonal mesh (1500 elements, 5254 edges, $h \approx 0.0268$). *Top*: Profiles of numerical velocity and pressure; *Bottom*: Streamlines and pressure field.

right of) the obstacle. The bottom panel shows the streamlines obtained from the numerical velocity. Clearly, the flow takes a detour around the obstacle and returns to its original path, e.g., a flow particle starts at $y = 0.45$ (when $x = 0$) returns to basically the same position $y = 0.45$ when $x = 1$. So our lowest-order WG method captures the main physical features of the flow.

We also comment that the posed velocity boundary conditions have discontinuity at the four corners and hence induce pressure singularity at those corners, but the streamlines (flow path) are actually not affected by such singularity.

Example 4 (*Flow Over a Backfacing Step*)**.** This is another benchmark problem that has been widely tested in the literature [16,25]. As shown in Fig. 5, the domain is $\Omega = ((-1, 5) \times (-1, 1)) \setminus (-1, 0)^2$. The body force is $\mathbf{f} = \mathbf{0}$ and $\mu = 1$. Dirichlet

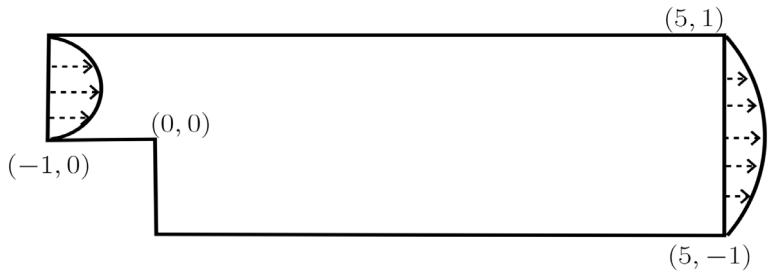

Fig. 5. Example 4 (Flow over a backfacing step): Problem description.

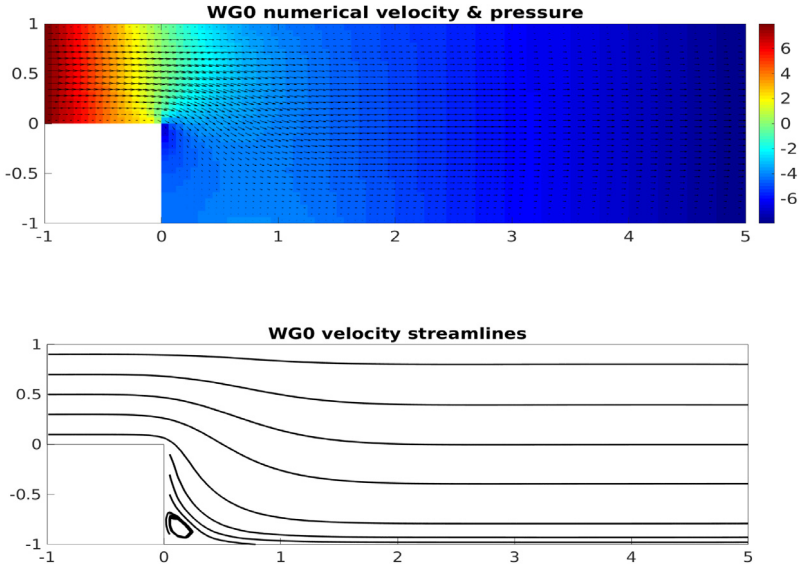

Fig. 6. Example 4 (Flow over a back step) simulated by WG on a rectangular mesh with 2304 elements, 5872 edges, and $h \approx 0.0570$.

boundary conditions are posed on the whole boundary. More specifically,

$$\mathbf{u}(x,y) = \begin{cases} [4(1-y)y, 0]^T & \text{for } x = -1,\ y \in (0,1), \\ [(1+y)(1+y)/2, 0]^T & \text{for } x = 5,\ y \in (-1,1), \\ \mathbf{0} & \text{for other parts of } \partial\Omega. \end{cases} \tag{94}$$

In other words, the fluid enters from the left boundary ($x = -1$) following a Poiseuille pattern and exits from the right boundary ($x = 5$) following a Poiseuille pattern also. At the entry, the maximum of u_1 is 1 and the total flux is 2/3. At the exit, the maximum of u_1 is 1/2 but the total flux is still 2/3. These make the total flux zero on the whole boundary.

We solve the problem using the lowest-order WG finite element method on a sequence of rectangular meshes. In Fig. 6, the top panel demonstrates the pressure drop right after the step corner; the bottom panel shows the eddy near the step bottom; all as expected.

8. Concluding remarks

In this paper, we have developed a simple new finite element method in the weak Galerkin framework for Stokes flow in two space dimensions. The method has some noticeable features.

(i) It is for polygonal meshes and hence includes triangular [16], rectangular, and quadrilateral meshes all as special cases.
(ii) It uses just constant vectors (in element interiors and on edges separately) for velocity approximation and constant scalars (on elements) for pressure approximation.
(iii) The method has expected 1st order accuracy in velocity and pressure.
(iv) The method is practically useful as demonstrated by numerical experiments on several widely tested benchmarks. It captures the main physical features and has the flexibility of using different types of meshes.

The method can be further reduced to a version using the discretely divergence-free subspace for velocity approximation. This results in a symmetric positive-definite linear system and hence overcomes the saddle-point problem. A subsequent pressure recovery procedure has also been established.

On the theoretical aspect, the identities on conversion to trace (Lemma 2) reveal the connection between the trace-interior difference and the discrete gradient/divergence of a discrete weak function. The matching between constant approximants for pressure and constants for discrete weak divergence of velocity allows us to establish stability for this new finite element method.

There are many directions one could go from here:

- A similar method for linear elasticity on polygonal meshes. Error analysis in the grad-div formulation is doable by using similar techniques in [11,14]. But an analysis in the strain-div formulation is challenging.
- Extension of the method to 3-dim or higher orders.

These are currently under our investigation and will be reported in our future work.

Acknowledgments

G. Harper and J. Liu were partially supported by US National Science Foundation under grant DMS-1819252. We thank Zhuoran (Sophy) Wang for her kind help on Figs. 1 and 5. We thank Dr. Lin Mu also for the stimulating discussion.

References

[1] H. Elman, D. Silverster, A. Wathen, Finite Elements and Fast Iterative Solvers, Oxford University Press, 2005.
[2] F. Brezzi, M. Fortin, Mixed and Hybrid Finite Element Methods, Springer-Verlag, 1991.
[3] M.D. Gunzburger, Finite Element Methods for Viscous Incompressible Flows: A Guide to Theory, Practice and Algorithms, Academic Press, San Diego, 1989.
[4] F. Thomasset, Implementation of Finite Element Methods for Navier-Stokes Equations, Springer-Verlag, Berlin, 1981.
[5] R. Rannacher, S. Turek, Simple nonconforming quadrilateral Stokes element, Numer. Math. 8 (2) (1992) 97–111.
[6] G. Lin, J. Liu, F. Sadre-Marandi, A comparative study on the weak Galerkin, discontinuous Galerkin, and mixed finite element methods, J. Comput. Appl. Math. 273 (2015) 346–362.
[7] J. Liu, F. Sadre-Marandi, Z. Wang, DarcyLite: A Matlab toolbox for Darcy flow computation, Procedia Comput. Sci. 80 (2016) 1301–1312.
[8] J. Liu, S. Tavener, Z. Wang, Lowest-order weak Galerkin finite element method for Darcy flow on convex polygonal meshes, SIAM J. Sci. Comput. 40 (2018) B1229–B1252.
[9] J. Wang, X. Ye, A weak Galerkin finite element method for second order elliptic problems, J. Comput. Appl. Math. 241 (2013) 103–115.
[10] J. Wang, X. Ye, A weak Galerkin mixed finite element method for second order elliptic problems, Math. Comp. 83 (2014) 2101–2126.
[11] S.-Y. Yi, A lowest-order weak Galerkin method for linear elasticity, J. Comput. Appl. Math. 350 (2019) 286–298.
[12] J. Wang, X. Ye, A weak Galerkin finite element method for the Stokes equations, Adv. Comput. Math. 42 (1) (2016) 155–174.
[13] R. Wang, X. Wang, Q. Zhai, R. Zhang, A weak Galerkin finite element scheme for solving the stationary Stokes equations, J. Comput. Appl. Math. 302 (2016) 171–185.
[14] G. Harper, J. Liu, S. Tavener, B. Zheng, Lowest-order weak Galerkin finite flement methods for elasticity on quadrilateral and hexahedral meshes, J. Sci. Comput. 78 (2019) 1917–1941.
[15] J. Liu, S. Tavener, Z. Wang, The lowest-order weak Galerkin finite element methods for the Darcy equation on quadrilateral and hybrid meshes, J. Comput. Phys. 359 (2018) 312–330.
[16] L. Mu, X. Ye, A simple finite element method for the Stokes equations, Adv. Comput. Math. (2017).
[17] W. Chen, Y. Wang, Minimal degree H(curl) and H(div) conforming finite elements on polytopal meshes, Math. Comp. 86 (2017) 2053–2087.
[18] E. Wachspress, Barycentric coordinates for polytopes, Comput. Math. Appl. 61 (2011) 3319–3321.
[19] M. Floater, A. Gillette, N. Sukumar, Gradient bounds for Wachspress coordinates on polytopes, SIAM J. Numer. Anal. 52 (2014) 515–532.
[20] D. Griffiths, A. Mitchell, Finite elements for incompressible flows, Math. Methods Appl. Sci. 1 (1) (1979) 16–31.
[21] R. LeVeque, High-resolution conservative algorithms for advection in incompressible flow, SIAM J. Numer. Anal. 33 (1996) 627–665.
[22] C. Talischi, G. Paulino, A. Pereira, I. Menezes, PolyMesher: a general-purpose mesh generator for polygonal elements written in Matlab, Struct. Multidiscip. Optim. 45 (2012) 309–328.
[23] J. Liu, Penalty-factor-free discontinuous Galerkin methods for 2-dim Stokes problems, SIAM J. Numer. Anal. 49 (2011) 2165–2181.
[24] J.-H. Chen, W. Pritchard, S. Tavener, Bifurcation for flow past a cylinder between parallel planes, J. Fluid Mech. 284 (1995) 23–41.
[25] M. Yang, J. Liu, Y. Lin, Pressure recovery for the weakly over-penalized discontinuous Galerkin methods for the Stokes problem, J. Sci. Comput. 63 (2015) 699–715.